Magnetism in spin models for depleted honeycomb-lattice iridates: Spin-glass order towards percolation

Eric C. Andrade
Institut für Theoretische Physik, Technische Universität Dresden, 01062 Dresden, Germany
and Instituto de Física Teórica, Universidade Estadual Paulista, Rua Dr. Bento Teobaldo Ferraz 271, Bl. II, 01140-070 São Paulo, SP, Brazil

Matthias Vojta
Institut für Theoretische Physik, Technische Universität Dresden, 01062 Dresden, Germany
(Received 24 September 2013; revised manuscript received 16 October 2014; published 7 November 2014)

Iridates are characterized by a fascinating interplay of spin-orbit and electron-electron interactions. The honeycomb-lattice materials A_2IrO_3 (A = Na,Li) have been proposed to realize pseudospin-1/2 Mott insulating states with strongly anisotropic exchange interactions, described by the Heisenberg-Kitaev model, but other scenarios involving longer-range exchange interactions or more delocalized electrons have been put forward as well. Here we study the influence of nonmagnetic doping, i.e., depleted moments, on the magnetic properties of experimentally relevant variants of the Heisenberg-Kitaev and Heisenberg J_1-J_2-J_3 models. We generically find that the zigzag order of the clean system is replaced, upon doping, by a spin-glass state with short-ranged zigzag correlations. We determine the spin-glass temperature as a function of the doping level and show that this quantity allows one to assess the importance of longer-range exchange interactions when the doping is driven across the site-percolation threshold of the honeycomb lattice.

DOI: 10.1103/PhysRevB.90.205112 PACS number(s): 75.10.Nr, 74.72.−h, 75.10.Jm, 75.50.Ee

I. INTRODUCTION

The interplay of strong spin-orbit coupling and electronic correlations is at the heart of many recent developments in condensed-matter physics, involving, e.g., correlated topological insulators, fractional Chern insulators, and spin-orbit Mott insulators [1–5]. On the materials side, oxides with partially filled 5d shells, such as iridates and osmates, are considered promising candidates in order to realize the theoretically proposed phenomena.

In this context, the insulating iridates A_2IrO_3 (A = Na,Li) have attracted enormous attention over the past few years [6–11]. In these materials, the Ir^{4+} ions are arranged in a layered honeycomb-lattice structure. Due to the combined effect of strong spin-orbit coupling and Coulomb interactions, the Ir $5d^5$ states, with one hole in the t_{2g} manifold, have been proposed to realize $J_{\rm eff} = 1/2$ spin-orbit Mott insulators [12,13], similar to other layered iridates [4,5]. Furthermore, Ref. [14] suggested that the magnetism of the $J_{\rm eff} = 1/2$ moments is dominated by strongly spin-anisotropic compass interactions, which by itself lead to the spin-liquid model on the honeycomb lattice proposed by Kitaev [15]. Supplemented by additional spin-isotropic Heisenberg interactions, the resulting Heisenberg-Kitaev (HK) model has been shown to host both spin-liquid and conventionally ordered phases [14,16–21].

Experimentally, both Na_2IrO_3 and Li_2IrO_3 have been found to undergo a magnetic ordering transition at $T_N \simeq 15$ K [6–8]. In Na_2IrO_3 the low-temperature spin configuration has been identified as collinear "zigzag" order [9,10], with ferromagnetic zigzag chains arranged antiferromagnetically in the honeycomb plane. This state is indeed a ground state of the HK model, where it results from a competition of antiferromagnetic Kitaev and ferromagnetic Heisenberg interactions [19]. Alternatively, Heisenberg and HK models with longer-range interactions have been considered: Specifically, a Heisenberg J_1-J_2-J_3 model with sizable second- and third-neighbor coupling has been found to describe the available data as well [9,22]. Finally, a more itinerant scenario in terms of molecular orbitals has also been proposed [23], although a detailed description of the magnetic properties in this model is lacking to date.

In this paper, we propose magnetic depletion, i.e., the random substitution of magnetic Ir^{4+} by nonmagnetic ions, as a powerful tool to study the magnetism of A_2IrO_3 and to discriminate between the various proposed scenarios for magnetism. A key insight is that, within local-moment models, depletion will inevitably turn the zigzag ordered state into a spin (or spin-orbit) glass: Both the HK and J_1-J_2-J_3 models are frustrated, and the combination of disorder and frustration generically causes spin-glass behavior [24]. We calculate the freezing temperature $T_g(x)$ as a function of doping level x and show that its behavior across the site-percolation threshold, $x_p = 30.3\%$, strongly differs between the HK and J_1-J_2-J_3 models (Fig. 1).

II. MODELS

We focus on two models which have been considered to describe the zigzag ordered state of Na_2IrO_3. The first is the HK model,

$$\mathcal{H} = J \sum_{\langle ij \rangle} \vec{S}_i \cdot \vec{S}_j + 2K \sum_{\langle ij \rangle_\gamma} S_i^\gamma S_j^\gamma , \qquad (1)$$

and the second is the J_1-J_2-J_3 model,

$$\mathcal{H} = J_1 \sum_{\langle ij \rangle} \vec{S}_i \cdot \vec{S}_j + J_2 \sum_{\langle\langle ik \rangle\rangle} \vec{S}_i \cdot \vec{S}_k + J_3 \sum_{\langle\langle\langle il \rangle\rangle\rangle} \vec{S}_i \cdot \vec{S}_l . \qquad (2)$$

Here, the sums run over pairs of nearest-, second-, and third-neighbor sites, respectively, while $\gamma = x,y,z$ in Eq. (1)

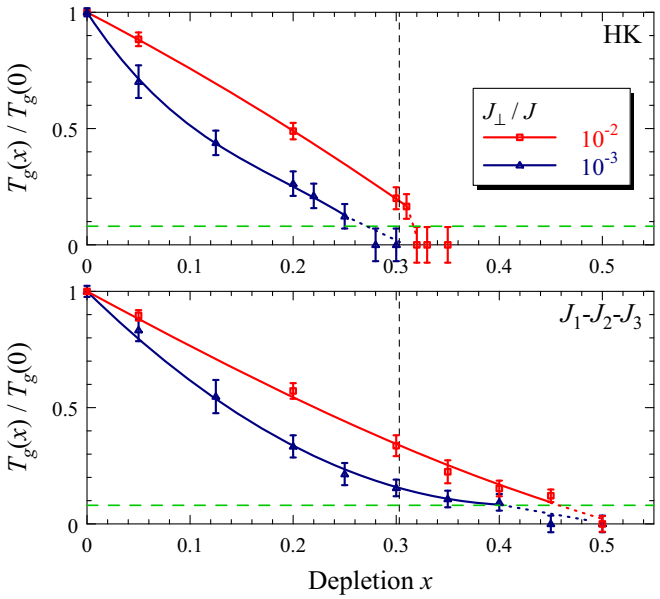

FIG. 1. (Color online) Freezing temperature extracted from our Monte Carlo (MC) simulations, shown as $T_g(x)/T_g(x=0)$ as a function of doping level x, for the HK (top) and J_1-J_2-J_3 (bottom) models for two different values of the interlayer coupling $J_\perp/J$. The vertical dashed line locates the two-dimensional (2D) percolation threshold x_p; the horizontal dashed line marks temperatures below which we are unable to reach equilibrium in our MC simulations. Solid lines are polynomial fits through the data; dotted lines are extrapolations.

labels the three different links for each spin in a honeycomb lattice. The parameter regimes of interest are defined through the presence of zigzag magnetic order as realized in Na_2IrO_3 [9,10]. The HK model's couplings may be parametrized as $J = A\cos\phi$ and $K = A\sin\phi$, where A is an overall energy scale. Its full phase diagram was first mapped out in Ref. [19], with the zigzag phase occurring for $0.51\pi < \phi < 0.90\pi$; in the following we choose $\phi = 0.62\pi$. For the J_1-J_2-J_3 model, sizable J_2 and J_3 are required in order to have a zigzag magnetic ground state [25–27]. Following Ref. [9], we choose $J_2 = 0.8J_1$ and $J_3 = 0.9J_1$.

As will become clear below, the magnetic properties of the depleted HK and J_1-J_2-J_3 models depend sensitively on the presence of a magnetic coupling between the layers. For A_2IrO_3, no quantitative information on such coupling is available at present; it is often assumed to be small due to the A-B-type stacking of the honeycomb layers. Here we will account for the three-dimensional (3D) character by considering a layered model with A-A stacking and a small vertical (unfrustrated) Heisenberg coupling $J_\perp$; in application to A_2IrO_3 this is to be understood as an effective coupling between second-neighbor layers.

III. MONTE CARLO SIMULATIONS

We study the models (1) and (2) using classical Monte Carlo (MC) simulations for unit-length spins on lattices of size $L \times L \times L_z$, typically with $L_z = L/2$ and periodic boundary conditions. The honeycomb layers are spanned by the primitive lattice vectors $\vec{a}_{1(2)} = (3/2, \pm\sqrt{3}/2)$, with each unit cell containing two sites. Depletion is simulated by randomly removing a fraction x of spins, with x varying between 5% and 50%, with the total number of spins $N_s = (1-x)2L^2L_z$. We perform equilibrium MC simulations using single-site updates with a combination of the heat-bath and microcanonical (or overrelaxation) methods, with typically 10^6 MC steps per spin, and combine this with the parallel-tempering algorithm [28,29]. Disorder averages are taken over $N_{\rm rl}$ samples, with $N_{\rm rl}$ ranging from 1000 for $L = 8$ to $N_{\rm rl} = 50$ for $L = 20$. Below we quote energies in units of $J \equiv J_1$, the nearest-neighbor Heisenberg exchange.

We extract the ordering (or freezing) temperature T_g from the crossing points of $\xi(T)/L$ for different L, according to the scaling law $\xi/L = f(L^{1/\nu}(T - T_g))$, where ξ is a correlation length, $f(x)$ a scaling function, and ν the correlation length exponent. This procedure is especially suitable to detect spin-glass freezing, as shown in previous studies of the 3D Edwards-Anderson model [30–32]. The main source of numerical error in T_g is from the $L \to \infty$ extrapolation of the crossing-point location required for small L.

The magnetic correlation length ξ_S is calculated from a fit of the static magnetic structure factor $S(\vec{q})$ close to the ordering wave vector $\vec{Q}$ [the three independent $\vec{Q}$ vectors corresponding to the zigzag order are $(\vec{b}_1 + \vec{b}_2)/2$, $\vec{b}_1/2$, and $\vec{b}_2/2$, where $\vec{b}_{1(2)} = 2\pi(1/3, \pm 1/\sqrt{3})$ are the reciprocal lattice vectors]. Analogously, the spin-glass correlation length ξ_{SG} is obtained from the spin-glass susceptibility $\chi_{SG}(\vec{q}) = N_s \sum_{\alpha,\beta}[\langle|q^{\alpha,\beta}(\vec{q})|^2\rangle]_{\rm avg}$, where $q^{\alpha,\beta}(\vec{q}) = N_s^{-1}\sum_i S_i^{\alpha(1)} S_i^{\beta(2)} \exp(i\vec{q}\cdot\vec{r}_i)$ is the spin-glass order parameter. Here α and β are spin components, superscripts (1,2) denote identical copies of the system ("replicas") containing the disorder configuration, $\langle\cdots\rangle$ denotes the MC average, and $[\cdots]_{\rm avg}$ the average over disorder.

IV. CLEAN HK MODEL

The 2D disorder-free HK model has been studied by various numerical methods [14,17,19–21]. A comparison of phase diagrams shows that the classical-spin HK model reproduces [21] all phases of the spin-1/2 model except for the quantum spin liquid [19], with $T = 0$ phase-boundary locations in reasonable agreement between quantum and classical models. The results in Refs. [20,21] also indicate two thermal transitions upon cooling to any of the ordered low-T phases. The system enters a critical phase at T_u, with power-law spin correlations, and a state with true long-range order is reached only below $T_l < T_u$. This behavior parallels that of a 2D six-state clock model [33], as suggested by the sixfold degeneracy of the ordered states in the HK model.

For selected values of ϕ, we have verified that our MC simulations, applied to the 2D HK model ($J_\perp = 0$), reproduce the results of Ref. [21]. In particular, the specific heat [Fig. 2(a)] shows a broad peak far above both T_u and T_l while the singularity at the transitions is weak—this reflects the presence of strong fluctuations in the 2D system. Nevertheless, there is a well-defined crossing point in ξ_S/L at T_l where long-range order sets in [Fig. 2(c)].

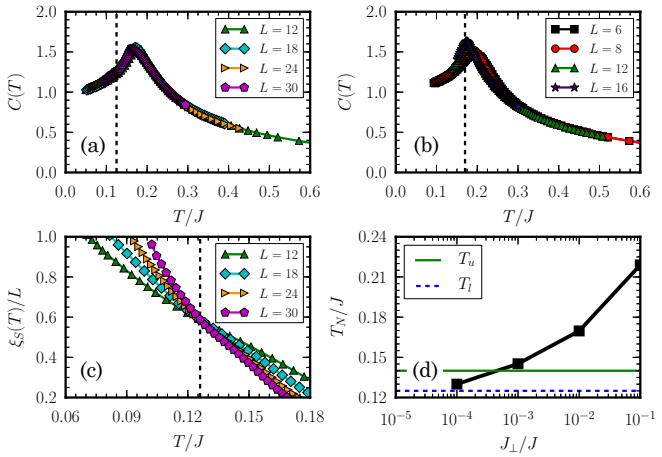

FIG. 2. (Color online) MC results for the ordering into the zigzag state of the clean HK model for several system sizes L. (a), (c) 2D. (b), (d) 3D. (a), (b) Specific heat as a function of the temperature T, in (b) with $J_\perp/J = 10^{-2}$. (c) ξ_S/L as a function of T. The vertical dashed line indicates T_l. (d) $T_N(J_\perp/J)$, also showing T_u and T_l of the 2D HK model; the value of T_u was extracted from Ref. [21].

We have then switched on the interlayer coupling $J_\perp$ and monitored the evolution of the transition temperature [Fig. 2(d)]. As expected on general grounds, the critical intermediate phase of the 2D system disappears for finite $J_\perp$, such that there is only a single thermal phase transition at T_N, which now displays a pronounced specific-heat singularity [Fig. 2(b)]. For $J_\perp/J \gtrsim 10^{-3}$, T_N is larger than both T_l and T_u of the 2D system, and our data are compatible with $T_N \to T_l$ as $J_\perp \to 0$, although finite-size effects hamper an accurate determination of T_N for $J_\perp/J < 10^{-4}$ [Fig. 2(d)].

Clean J_1-J_2-J_3 model. We have also performed corresponding simulations for the J_1-J_2-J_3 model. Here, $T_N \to 0$ for $J_\perp \to 0$ due to the assumed continuous spin symmetry. For $J_\perp/J = 10^{-2}$ [10^{-3}] we have $T_N/J = 0.446(3)$ [0.42(1)].

V. MAGNETIC DEPLETION

We now describe our central results, obtained for the depleted HK and J_1-J_2-J_3 models, with a concentration x of randomly placed vacancies. Since both models are frustrated, the introduction of vacancies generate local noncollinearities in the spin order [34], which ultimately leads to spin-glass behavior [24].

We have first studied the 2D case ($J_\perp = 0$) and found—in both models and for any $x \geqslant 5\%$—indications of neither conventional nor spin-glass order at finite temperature. This is expected: Conventional order is suppressed, due to the combination of disorder and frustration, in favor of spin-glass magnetism. However, the glass temperature is strictly zero in two dimensions [35,36], even in the case of Ising symmetry.

For finite interlayer coupling the situation changes, with sample results shown in Fig. 3. While conventional long-range order is absent for any $x \geqslant 5\%$, spin-glass order emerges instead at low T. The latter is signified by a well-defined common crossing point in ξ_{SG}/L and a corresponding scaling [Figs. 3(c) and 3(d)] [37]. In contrast, existing crossing points of ξ_S/L display a systematic downward shift with increasing L,

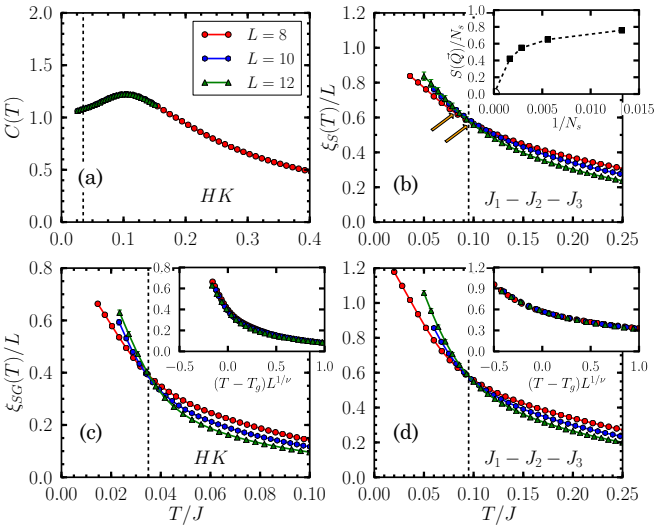

FIG. 3. (Color online) MC results for the ordering into the spin-glass state for $J_\perp/J = 10^{-2}$. (a), (c) HK model at $x = 30\%$. (b), (d) J_1-J_2-J_3 model at $x = 35\%$. (a) Specific heat as a function of the temperature T. (b) ξ_S/L as a function of T. The arrows indicate the crossing points of the curves for different pairs of L, displaying a clear downward trend with increasing L. Inset: Bragg intensity $S(\tilde{Q}/N_s)$ extrapolated to $T \to 0$ as a function of $1/N_s$. (c), (d) ξ_{SG}/L as a function of T. Inset: Scaling plot with ξ_{SG}/L as a function of $(T - T_g)L^{1/\nu}$. The vertical dashed lines indicate the glass temperature T_g, as determined in (c) and (d).

indicative of short-range zigzag spin correlations [Fig. 3(b)]. We note that we do not reach the limit $L \gg \xi_S(T = 0)$ where crossing points would be absent entirely.

Short-range magnetic order also manifests itself in the specific heat [Fig. 3(a)]. The peak in $C(T)$ is broad and occurs at a temperature considerably larger than the freezing temperature (here $T_{peak} \approx 2T_g$), indicating that this short-range order builds up at temperatures considerably higher than T_g. We stress that this behavior is a hallmark of glassy systems [29,36], and it is, in principle, disconnected from the nontrivial behavior of the 2D disorder-free HK model [20] [Fig. 2(a)].

To account for the possibility of different (non-zigzag) dilution-induced magnetic ground states, we monitored $S(\vec{q})$ in the reciprocal space, but (within our resolution) we detected peaks only at the $\tilde{Q}$ vectors corresponding to the zigzag order. However, these peaks grow slower than the system size [Fig. 3(b)], again indicating static short-range order with a vanishing magnetic order parameter.

VI. SMALL DOPING AND GLASSINESS

In both the Heisenberg-Kitaev and J_1-J_2-J_3 models, we find a single vacancy to produce anticollinear states [34]. Multiple vacancies have a somewhat different effect in the two models: In the Heisenberg-Kitaev case, the vacancies locally select specific stripe orientations due to spin-orbit coupling [38], causing domains with different stripe orientations to coexist. In the J_1-J_2-J_3 model, instead, the effect of long-range distortions of the spin pattern is more prominent, due to the presence of gapless bulk modes. Remarkably, for the vacancy concentrations of interest, $x \geqslant 20\%$, the spin configurations

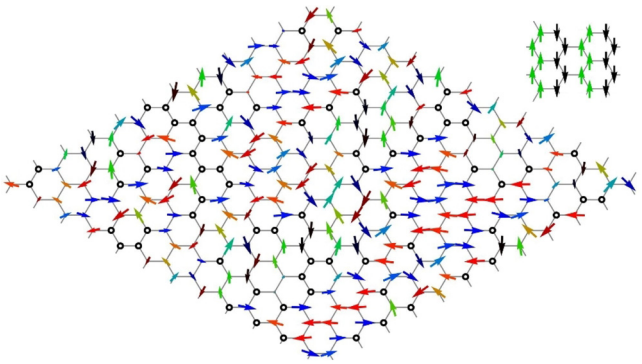

FIG. 4. (Color online) Sample ground-state spin configuration of the classical HK model at $x = 20\%$ depletion, with one $L = 12$ layer shown. The arrows denote the x and z components of the $\vec{S}_i$; the circles indicate the vacancy positions. The arrow lengths indicate the weight of the projection onto the x-z plane and the colors the in-plane orientation. Short-range zigzag order with glassy domain formation is visible. Inset: Ideal zigzag order with the spins aligned along S_i^z.

we observe in both models are virtually indistinguishable and are characterized by a short-range domain structure (Fig. 4).

Based on our MC data, we are unable to decide whether long-range order is destroyed in favor of spin-glass order at infinitesimal x or at a finite critical x_c (with $x_c < 5\%$). We leave a more detailed characterization of the small-doping behavior for future work.

VII. ORDERING TEMPERATURE AND PERCOLATION

An easily accessible quantity is the ordering (or freezing) temperature T_g as function of x. While one generally expects that T_g decreases with increasing x, the behavior at large x contains information on the nature of the magnetic couplings: For a layered local-moment system with nearest-neighbor couplings, T_g will diminish near the threshold x_p for 2D site percolation, because for $x > x_p$ the layers fragment into disconnected spin clusters, and for Heisenberg symmetry $T_g(x)/T_g(x=0)$ will vanish as $x \to x_p$ in the limit of small interlayer coupling. In contrast, in systems with longer-range magnetic couplings, T_g will stay finite across x_p [39]. The parent compounds of cuprate superconductors exemplify this physics: The Néel temperature in Zn-doped La_2CuO_4 vanishes essentially at the square-lattice percolation threshold of $x_p = 40.5\%$ [40]—this proves that the cuprate magnetism is dominated by nearest-neighbor coupling.

Our results for $T_g(x)$ are shown in Fig. 1. As expected from the above discussion, T_g of the nearest-neighbor HK model rapidly drops towards the honeycomb lattice $x_p = 30.3\%$ and becomes smaller than our lowest simulation temperature ($J/80$) for $x \gtrsim 32\%$ for $J_\perp/J = 10^{-2}$. (Note that, due to the finite $J_\perp$, T_g is expected to be nonvanishing up to the 3D percolation threshold, however, it is undetectably small for $x \gtrsim 32\%$.) For smaller interlayer coupling this apparent vanishing of $T_g(x)$ appears at even smaller x.

In contrast, T_g of the J_1-J_2-J_3 model continues its approximately linear variation with x across x_p and extrapolates to our lowest simulation temperature at a much larger doping level of $x \approx 50\%$ [41]. For both models, $T_g(x)/T_g(x=0)$ diminishes with decreasing $J_\perp/J$, and small $J_\perp/J$ induce a curvature in $T_g(x)$, which is particularly pronounced at small x.

VIII. SUMMARY

We have studied the magnetism of local-moment models for A_2IrO_3 under magnetic depletion. A spin-orbit glass, with zigzag short-range order, emerges generically from the combination of strong spin-orbit coupling, frustration, and disorder. We have determined the glass (or freezing) temperature T_g as a function of the doping level x, which at large doping differs qualitatively between the HK and J_1-J_2-J_3 models [Fig. 1(a)].

We thus propose to employ magnetic depletion, using dopants with magnetically inert d shells, as a tool to assess the importance of longer-range magnetic couplings in the A_2IrO_3 compounds: If the experimental T_g were found to vanish near x_p, this would strongly hint [42] at short-range HK physics being realized in A_2IrO_3, as originally proposed in Refs. [14,19]. Conversely, the absence of such vanishing would imply significant longer-range interactions.

Note added. Very recent experiments [43], using nonmagnetic Ti dopants substituting for Ir, show significant differences between depleted Na_2IrO_3 and Li_2IrO_3 across the percolation threshold.

ACKNOWLEDGMENTS

We thank J. van den Brink, P. Gegenwart, P. Horsch, G. Khaliullin, and A. Rosch for discussions. The computations were partially performed at the Center for Information Services and High Performance Computing (ZIH) at TU Dresden. This research was supported by the DFG through FOR 960 and GRK 1621 as well as by the Helmholtz association through VI-521. E.C.A. was also partially supported by FAPESP (Brazil).

[1] D. A. Pesin and L. Balents, Nat. Phys. **6**, 376 (2010).
[2] M. Hohenadler and F. F. Assaad, J. Phys.: Condens. Matter **25**, 143201 (2013).
[3] E. J. Bergholtz and Z. Liu, Int. J. Mod. Phys. B **27**, 1330017 (2013).
[4] B. J. Kim, H. Jin, S. J. Moon, J.-Y. Kim, B.-G. Park, C. S. Leem, J. Yu, T. W. Noh, C. Kim, S.-J. Oh, J.-H. Park, V. Durairaj, G. Cao, and E. Rotenberg, Phys. Rev. Lett. **101**, 076402 (2008).
[5] B. J. Kim, H. Ohsumi, T. Komesu, S. Sakai, T. Morita, H. Takagi, and T. Arima, Science **323**, 1329 (2009).
[6] Y. Singh and P. Gegenwart, Phys. Rev. B **82**, 064412 (2010).
[7] X. Liu, T. Berlijn, W.-G. Yin, W. Ku, A. Tsvelik, Y.-J. Kim, H. Gretarsson, Y. Singh, P. Gegenwart, and J. P. Hill, Phys. Rev. B **83**, 220403 (2011).
[8] Y. Singh, S. Manni, J. Reuther, T. Berlijn, R. Thomale, W. Ku, S. Trebst, and P. Gegenwart, Phys. Rev. Lett. **108**, 127203 (2012).

[9] S. K. Choi, R. Coldea, A. N. Kolmogorov, T. Lancaster, I. I. Mazin, S. J. Blundell, P. G. Radaelli, Y. Singh, P. Gegenwart, K. R. Choi, S.-W. Cheong, P. J. Baker, C. Stock, and J. Taylor, Phys. Rev. Lett. **108**, 127204 (2012).

[10] F. Ye, S. Chi, H. Cao, B. C. Chakoumakos, J. A. Fernandez-Baca, R. Custelcean, T. F. Qi, O. B. Korneta, and G. Cao, Phys. Rev. B **85**, 180403 (2012).

[11] R. Comin, G. Levy, B. Ludbrook, Z.-H. Zhu, C. N. Veenstra, J. A. Rosen, Y. Singh, P. Gegenwart, D. Stricker, J. N. Hancock, D. van der Marel, I. S. Elfimov, and A. Damascelli, Phys. Rev. Lett. **109**, 266406 (2012).

[12] G. Jackeli and G. Khaliullin, Phys. Rev. Lett. **102**, 017205 (2009).

[13] A. Shitade, H. Katsura, J. Kuneš, X.-L. Qi, S.-C. Zhang, and N. Nagaosa, Phys. Rev. Lett. **102**, 256403 (2009).

[14] J. Chaloupka, G. Jackeli, and G. Khaliullin, Phys. Rev. Lett. **105**, 027204 (2010).

[15] A. Kitaev, Ann. Phys. (NY) **321**, 2 (2006).

[16] H.-C. Jiang, Z.-C. Gu, X.-L. Qi, and S. Trebst, Phys. Rev. B **83**, 245104 (2011).

[17] J. Reuther, R. Thomale, and S. Trebst, Phys. Rev. B **84**, 100406 (2011).

[18] S. Bhattacharjee, S.-S. Lee, and Y. B. Kim, New J. Phys. **14**, 073015 (2012).

[19] J. Chaloupka, G. Jackeli, and G. Khaliullin, Phys. Rev. Lett. **110**, 097204 (2013).

[20] C. C. Price and N. B. Perkins, Phys. Rev. Lett. **109**, 187201 (2012).

[21] C. C. Price and N. B. Perkins, Phys. Rev. B **88**, 024410 (2013).

[22] I. Kimchi and Y.-Z. You, Phys. Rev. B **84**, 180407 (2011).

[23] I. I. Mazin, H. O. Jeschke, K. Foyevtsova, R. Valenti, and D. I. Khomskii, Phys. Rev. Lett. **109**, 197201 (2012).

[24] J. Villain, Z. Phys. B **33**, 31 (1979).

[25] E. Rastelli, A. Tassi, and L. Reatto, Physica B+C **97**, 1 (1979).

[26] J. Fouet, P. Sindzingre, and C. Lhuillier, Eur. Phys. J. B **20**, 241 (2001).

[27] P. H. Y. Li, R. F. Bishop, D. J. J. Farnell, and C. E. Campbell, Phys. Rev. B **86**, 144404 (2012).

[28] For further details, see Ref. [29].

[29] E. C. Andrade and M. Vojta, Europhys. Lett. **97**, 37007 (2012).

[30] L. W. Lee and A. P. Young, Phys. Rev. Lett. **90**, 227203 (2003).

[31] I. Campos, M. Cotallo-Aban, V. Martin-Mayor, S. Perez-Gaviro, and A. Tarancon, Phys. Rev. Lett. **97**, 217204 (2006).

[32] D. X. Viet and H. Kawamura, Phys. Rev. Lett. **102**, 027202 (2009).

[33] J. V. Jose, L. P. Kadanoff, S. Kirkpatrick, and D. R. Nelson, Phys. Rev. B **16**, 1217 (1977).

[34] C. L. Henley, Phys. Rev. Lett. **62**, 2056 (1989).

[35] A. J. Bray and M. A. Moore, J. Phys. C **17**, L463 (1984).

[36] K. H. Fischer and J. A. Hertz, *Spin Glasses* (Cambridge University Press, Cambridge, UK, 1991).

[37] For both models, we estimate the same correlation length exponent $\nu \approx 1.05$. Due to our modest system sizes, we do not pursue a complete characterization of the critical exponents.

[38] F. Trousselet, G. Khaliullin, and P. Horsch, Phys. Rev. B **84**, 054409 (2011).

[39] A lattice with further-neighbor links has a larger site-percolation threshold than the one with nearest-neighbor links only.

[40] O. P. Vajk, P. K. Mang, M. Greven, P. M. Gehring, and J. W. Lynn, Science **295**, 1691 (2002).

[41] A honeycomb lattice with only J_2 couplings nonzero corresponds to two decoupled triangular lattices; the site-percolation threshold of a *triangular* lattice is $x = 50\%$.

[42] In more itinerant scenarios of A_2IrO_3 magnetism, such as in Ref. [23], site percolation is not expected to drastically influence $T_g(x)$.

[43] S. Manni, Y. Tokiwa, and P. Gegenwart, Phys. Rev. B **89**, 241102(R) (2014).